ChemComm

Accepted Manuscript

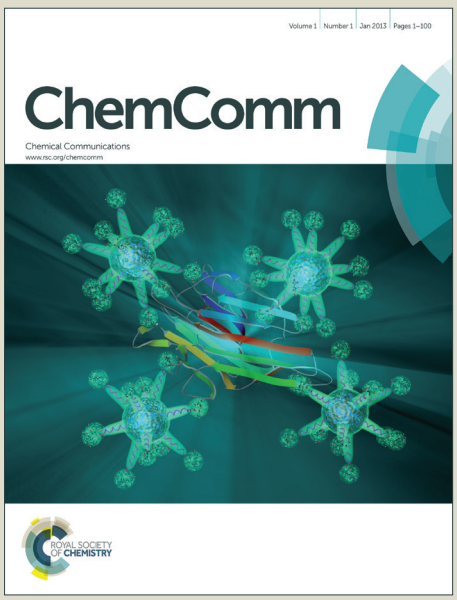

ROYAL SOCIETY OF CHEMISTRY

www.rsc.org/chemcomm

Journal Name

RSCPublishing

COMMUNICATION

Detection of nitroaromatic vapours with diketopyrrolopyrrole thin films: Exploring the role of structural order and morphology on thin film properties and fluorescence quenching efficiency

Cite this: DOI: 10.1039/x0xx00000x

Received 00th January 2012,
Accepted 00th January 2012

DOI: 10.1039/x0xx00000x

www.rsc.org/

Monika Warzecha,[a] Jesus Calvo-Castro,[a] Alan R. Kennedy,[b] Alisdair Macpherson,[c] Kenneth Shankland,[d] Norman Shankland,[e] Andrew J. McLean[a*] and Callum J. McHugh[a*]

Sensitive optical detection of nitroaromatic vapours with diketopyrrolopyrrole thin films is reported for the first time and the impact of thin film crystal structure and morphology on fluorescence quenching behaviour demonstrated.

Novel approaches to detection and identification of explosives is a field of significant worldwide importance.[1] To combat modern day global uncertainties, detection systems should be simple, inexpensive, robust and able to quickly identify a diversity of species.[2] Significant progress has been made in optical based methods and recent reviews highlight that this area shows great promise for future developments.[3,4] To date the most successful strategies are based upon solid state fluorescent materials and modulation of analyte response via electron transfer. Ubiquitous in this field are conjugated polymers developed by the Swager group and commercialised in the Fido® XT system.[4,5] Despite significant advances, improvements in sensor cost, adaptability, portability, size and complexity would be major innovations that could be realised via development of new optical and electronic based materials and technologies.[6]

In this regard, we are engaged in development of diketopyrrolopyrrole (DPP) small molecule semiconductors and recently reported high computed charge transfer integrals in DPP motifs displaying cofacial π-stacking in the solid state.[7] These derivatives and structural analogues also exhibit solid state emission and display high light and thermal fastness. Thus, they make promising candidates as signal transducers in *both* optical and electronic sensing environments. We report herein, for the first time, the *optical* behaviour of two DPP architectures whose solutions and thin films undergo effective fluorescence quenching upon exposure to nitroaromatics such as 2,4,6-trinitrotoluene (TNT), 2,4-dinitrotoluene (DNT) and nitrobenzene (NB). Crucially, the solid state vapour response towards these important targets is shown to be strongly influenced by the solid state structure and morphology of the DPP thin film environment.

We report optimal DPP structures as **HBDPP** and **BBDPP**, which were prepared as outlined in (Scheme 1).

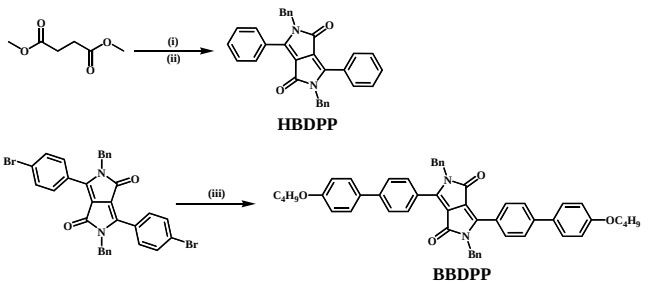

Scheme 1 (i) PhCN, Na, t-amyl alcohol, 120 °C; (ii) BnBr, K_2CO_3, DMF, 120 °C; (iii) $Pd(OAc)_2$, SPhos, 4-butoxyphenylboronic acid, K_3PO_4, THF

As reported by us previously, the single crystal structure of **HBDPP** is dominated by a long molecular axis, slipped (4.50 Å) cofacial π-π stacking arrangement along the crystallographic *a*-axis.[7] A single crystal structure of **BBDPP** was herein obtained to rationalise packing effects on its thin film properties and quenching performance (SI.2). The structure of **BBDPP** is consistent with **HBDPP** with a slipped cofacial stacking arrangement. In **BBDPP** however, the phenyl torsion is increased to 29 ° (c.f. 20 ° in **HBDPP**) and the long axis slip in the centrosymmetric monomer pairs reduced to 3.45 Å along the crystallographic *b*-axis. Accordingly, we propose given the presence of the cofacial intermolecular interactions that optical behaviour of both single crystals should be consistent with H-aggregates.[8] Optical and electrochemical data in dichloromethane solution and from bulk material in the solid state are collated in (SI.3). Solution absorption spectra for both DPPs were broad with no vibronic structure; the bathochromic shift of λ_{max} in **BBDPP** attributed to phenyl versus H-substitution. Fluorescence emission spectra in solution for each were also similar, with resolved vibronic structure observed. Solution

fluorescence quantum yields ϕ_F, were high for **HBDPP** and **BBDPP** (0.85 and 0.81 respectively) and insensitive to oxygen quenching under aerated conditions, greatly enhancing their potential application in working environments. Kubelka-Munk derived absorption spectra of both powders were broad and hypsochromically shifted compared to solution; a reduction in the absorption maximum in the solid state compared with solution (439 nm vs. 464 nm and 471 nm vs. 492 nm for **HBDPP** and **BBDPP** respectively) consistent with the blue shift expected from cofacial H-aggregates. Solid state fluorescence emission spectra of **HBDPP** and **BBDPP** were red shifted compared to solution (612 nm vs. 524 nm and 635 nm vs. 561 nm respectively), however from thin film data (*vide infra*) the large Stoke's shift in the powders is consistent with self-absorption.

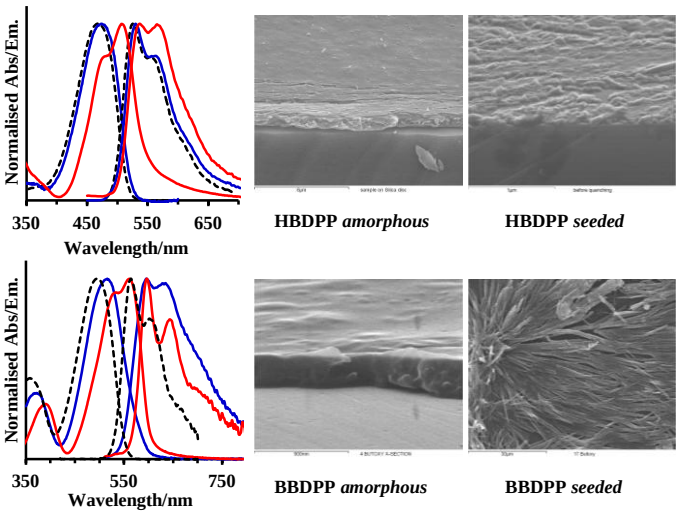

Fig. 1 **HBDPP** (top) and **BBDPP** (bottom) absorption and emission spectra from solution (black dash), amorphous (blue) and seeded thin films (red). SEM images of amorphous and seeded **HBDPP** and **BBDPP** films

Steady state fluorescence emission from **HBDPP** and **BBDPP** in dichloromethane was quenched upon exposure to NB, DNT and TNT under aerated conditions (SI.4). From fluorescence lifetimes (6.46 ns for **HBDPP** and 3.95 ns for **BBDPP**) and Stern-Volmer analysis, bimolecular rate constants for S_1 quenching k_q, (3.87 x 10^9, 7.72 x 10^9 and 1.26 x 10^{10} $M^{-1}s^{-1}$ for **HBDPP** and 3.37 x 10^9, 9.62 x 10^9 and 1.17 x 10^{10} $M^{-1}s^{-1}$ for **BBDPP** with NB, DNT and TNT respectively) were determined and found to approach the calculated diffusion controlled rate limit (SI.4); increases in k_q being consistent with increased quencher reduction potential. The Stern-Volmer plots were strictly linear in all cases with no change in DPP absorption spectra at high quencher concentration. Oxidation and reduction potentials of **HBDPP**, **BBDPP** and the nitroaromatics were determined by cyclic voltammetry. Calculation of ΔG (-0.103, -0.317 and -0.562 eV for **HBDPP** and -0.070, -0.285 and -0.530 eV for **BBDPP** with NB, DNT and TNT respectively) clearly indicating that in solution electron transfer is thermodynamically favourable from DPP S_1 to the nitroaromatic in all cases (SI.4).

Fluorescent thin films of **HBDPP** and **BBDPP** were prepared on SiO_2 by spin coating from dichloromethane. Film thickness determined by surface profiling was shown to correlate well to absorbance (SI.5). Amorphous films of **HBDPP** and **BBDPP** were prepared from filtered dye solutions and characterised by SEM and absorption and emission spectra, which for **HBDPP** were almost identical to those observed in solution (Fig. 1). Structured **HBDPP** films exhibiting higher long range order were obtained via seeding during spin coating; SEM analysis of these films showing nanocrystalline islands of the dye (Fig. 1). Enhanced order in seeded **HBDPP** films was supported by analysis of their absorption and emission spectra, which were red-shifted compared to the amorphous films as a result of solution-to-crystal effects and molecular planarisation. Both spectra exhibited characteristic vibronic ratio changes indicative of excitonic coupling (Fig. 1); increased intensity of the 0-1 transition in the absorption and emission spectra with respect to the 0-0 band supporting the presence of an H-aggregate and a structure consistent with that observed in the single crystal (*vide infra*).[8] Amorphous **BBDPP** films were characterised by instability, with conversion of their absorption and emission spectra to those of the seeded **BBDPP** films upon thermal or solvent annealing; the broad structureless absorption at 516 nm in the amorphous film undergoing an evolution to a vibronically resolved envelope with 0-0 and 0-1 bands centred at 561 nm and 535 nm respectively. The associated fluorescence emission 0-0 and 0-1 bands also exhibited an evolution from 597 and 628 nm in the amorphous **BBDPP** film to 597 and 643 nm in the seeded, more crystalline environment. Of key importance is the emergence of vibronic structure in the absorption and emission spectra consistent with the presence of J-aggregation in the seeded film; where the 0-0 band is more intense than the 0-1 in the absorption and emission spectra (Fig. 1).[8] It is noteworthy, that two quite different behaviours are apparent in the structure of thin films being produced; in the case of **HBDPP**, H-aggregate seeding ultimately gives rise to crystalline H-aggregate thin films. On the other hand, for **BBDPP**, both amorphous *and* H-aggregate seeding lead to a crystalline *J-aggregate* thin film structure which is consistent with polymorphism in this system. While noteworthy, this is not necessarily surprising based on our recent observations that N-benzyl DPPs may adopt various slipped cofacial orientations over their long molecular axis; with α and β polymorphs of chloro-substituted N-benzyl DPPs displaying J and H-aggregate π-π stacking motifs respectively.[7]

Quenching of thin film emission was investigated using a modified version of the method reported by Swager (SI.5).[4,5] Exposure of amorphous films of **HBDPP** to vapours of NB or DNT (a headspace marker for TNT)[9] gave complete reduction of fluorescence intensity with the time taken to reach maximum quenching dictated by film thickness, accessibility of largely monomeric emissive sites in these films and the quencher vapour pressure (Fig. 2a&b). Accordingly, rapid and complete quenching from 100 nm thick amorphous films of **HBDPP** fluorescence by NB was achieved after only 9 minutes, highlighting the efficient quenching in these films (Fig. 2a). For DNT, the dependence of film thickness on quenching rate was similarly observed, although in this case the overall quenching process was slower and consistent with the lower vapour pressure of DNT compared with NB (180 ppb vs. 300 ppm at

25 °C respectively).[5] Only 20 % of the total **HBDPP** emission was quenched after 9 minutes for a 180 nm thick film (100 % quenching being observed after prolonged exposure to DNT).

For amorphous **BBDPP** films a similar relationship was observed between NB and DNT quenching; NB producing a more rapid reduction in emission. However, for these films the time taken to reach quenching saturation was longer than for **HBDPP** films and the relationship between film thickness and quenching rate was reversed (SI.5). Moreover, and quite contrary to amorphous **HBDPP** films, exposure of amorphous **BBDPP** films to NB or DNT vapour also produced large changes in their absorption and emission spectra, associated with a change in film structure to the proposed J-aggregate conformation (SI.5). Thus, amorphous **BBDPP** films were not considered to be suitable as stable nitroaromatic sensing platforms as reduction in fluorescence emission could not be attributed *purely* to a quencher-fluorophore interaction. In contrast, seeded **BBDPP** films were *stable* to both NB and DNT vapours with no change in their absorption or emission spectral profiles (SI.5). Exposure to NB and DNT gave rapid reduction of film fluorescence with comparable performance to that reported previously in other systems[3,4,10,11] (Fig. 2d). For 100 nm thick films, over 30 % of the total emission intensity was quenched within 2 minutes of exposure to NB vapour. With DNT, a greater degree of overall quenching was observed (45 % at saturation) although the quenching rate was lower compared to NB (15 % quenched after 2 minutes). The difference in total fluorescence quenching is likely due to the increased reduction potential and enhanced electron transfer rate constant of DNT versus NB with the **BBDPP** seeded film. We propose this occurs via π-π interactions reported previously between DNT and aromatic systems.[3] The time taken to reach saturation of fluorescence quenching reflects the lower vapour pressure and hence pre-saturation concentration of available DNT quenchers compared to NB. In either case, the excellent response of seeded **BBDPP** thin films may be rationalised based on their J-aggregate film structure and fibrous morphology.[11]

Seeded **HBDPP** thin films were characterised by inherently slower response to nitroaromatic vapours compared to amorphous equivalents (Fig. 2a). After DNT exposure, 80 % of the total emission was quenched, compared to 100 % of emission in the amorphous film at maximum saturation time. This effect can be accounted for based on the more negative Δ*G* for electron transfer in the amorphous film which exhibits a blue shifted $E_{0\text{-}0}$ energy relative to the seeded film. The dramatic difference in the saturation times (756 minutes versus 200 minutes to achieve a 50 % reduction of emission intensity) in these systems reflects the greater accessibility of fluorescent species to DNT vapour in the amorphous film versus the more ordered seeded film environment. For NB quenching of seeded **HBDPP** films the situation was more complex; again we found clear evidence of a solvent annealing effect altering crystal morphology in the thin film confirmed by SEM and X-ray diffraction (XRD) analysis (Fig. 2c). The changes to fluorescence emission upon exposure to NB in this case must also be interpreted carefully, as they may originate through changes to film morphology and *not* electron transfer between the seeded **HBDPP** film and NB (SI.5.).

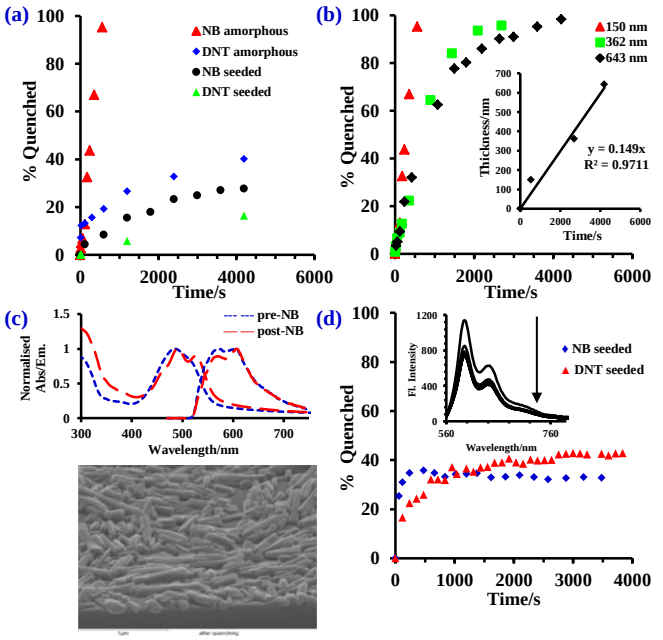

Fig. 2 a) Fluorescence quenching as a function of time for amorphous and seeded **HBDPP** films exposed to DNT and NB vapour b) effect of film thickness on rate of NB quenching for amorphous **HBDPP** films c) effect of NB exposure on absorption, emission and morphology of seeded **HBDPP** films d) fluorescence quenching as a function of time for seeded **BBDPP** films exposed to DNT and NB

To probe the effects of post deposition solvent annealing on structure, morphology and fluorescence quenching, seeded **HBDPP** films were exposed to acetone or toluene vapour. This afforded *stable* self-assembled microcrystals of **HBDPP** on the SiO_2 substrates similar to those observed after NB treatment (Fig. 3b). XRD analysis revealed reflections from 00*1*, 0*1*0 and 0*2*0 planes in films prepared on scattering SiO_2 treated with acetone or toluene (SI.6), whilst on non-scattering SiO_2 a preferred 00*l* progression was observed with reflections from 00*1*, 00*2*, 00*3*, 00*5* and 00*7* planes detected (Fig. 3a); both sets of XRD data confirmed via comparison with bulk powder and predicted powder X-ray diffraction (PXRD) patterns computed by Mercury[12] for the **HBDPP** single crystal (SI.6). For these **HBDPP** films, enhanced vibronic structure in the absorption spectra and emergence of a band at 463 nm, accompanied by an increase in the relative intensity of fluorescence at 606 nm is consistent with H-aggregate formation[8] (Fig. 3c). Accordingly, we propose that acetone and toluene annealed thin films of **HBDPP** are characterised by a structure consistent with the single crystal. Given that *h*00 planes from the crystal structure of **HBDPP** along the π-stacking *a*-axis are absent in the film XRDs implies that the needle like crystals observed by SEM (Fig. 3b) are orientated with the π-stacking *a*-axis parallel to the substrate and directed along the long dimension in the crystal aspect (SI.6). Thus, **HBDPP** solvent annealed films could exhibit promising *optoelectronic* sensing properties, with efficient charge transport in electronic devices observed from cofacial π-stacking along the current direction in the conducting channel.[13] Acetone and

toluene treatment of seeded **BBDPP** films also enhanced their crystallinity, confirmed by XRD and SEM, with very small changes observed in optical spectra (SI.6). In contrast to **HBDPP** however, diffraction data was not consistent between annealed **BBDPP** films, powder and single crystal, with the film optical spectra supporting a new crystal phase exhibiting the proposed J-aggregate structure (SI.6).

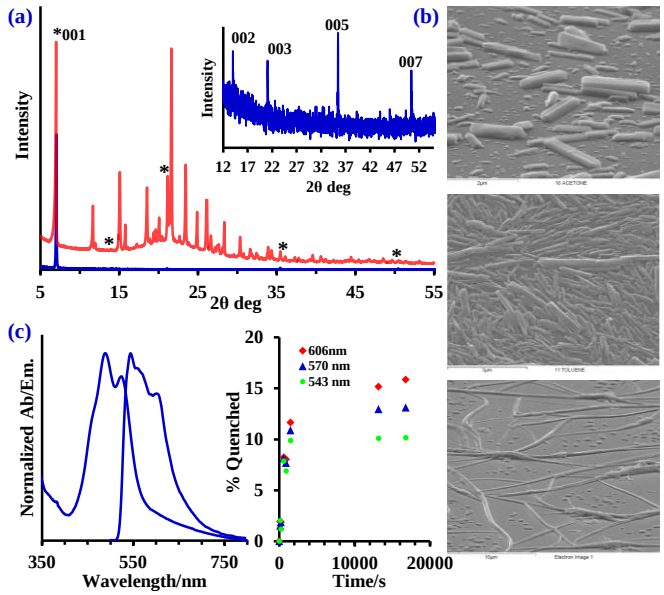

Fig. 3 a) PXRD pattern for **HBDPP** powder (red) and XRD pattern for acetone-annealed film (blue) with inset showing film 00/ progression (common reflections indicated by *) b) SEM images of acetone (top) and toluene (middle) annealed films of **HBDPP** and acetone-annealed film of **BBDPP** (bottom) c) absorption and emission spectra of toluene-annealed **HBDPP** film (left) and fluorescence quenching as a function of time for a 150 nm toluene-annealed **HBDPP** film exposed to DNT vapour (right)

Fluorescence from 150 nm thick toluene annealed films of **HBDPP** exposed to DNT and NB vapour was quenched by 10-15 %, reaching saturation after 280 and 60 minutes respectively. The increased time to reach maximum quenching for DNT again reflected its lower vapour pressure compared to NB. Reduction in total fluorescence quenching in these stable crystalline films with DNT and NB was consistent with slightly less favourable Δ*G* for electron transfer than seeded films but was dominated by decreased film surface area and accessible quenchable sites. From the surface area of crystallites determined by SEM analysis of acetone-annealed **HBDPP** films we propose that the π-stacking end faces of the crystals contribute on average to 7-8 % of the total crystal surface area in the chosen population (SI.6). Comparable reduction in emission intensity in crystalline **HBDPP** films may be attributed to a π-π interaction between these π-stacks and the nitroaromatic, also consistent with the larger reduction in intensity at saturation of H-aggregate emission at 606 nm compared to the bands at 570 nm and 543 nm (Fig. 3c). In toluene and acetone-annealed **BBDPP** films, DNT and NB quenching gave a rapid rise to saturation although the total quenching was less than with seeded films (SI.6). In these crystalline **BBDPP** environments, comparable Δ*G* for electron transfer with seeded equivalents infers that the difference in total fluorescence quenching between DNT and NB (20 % *vs*. 10 % overall) is consistent with quencher reduction potential. The overall reduction in total quenching for DNT and NB with these films is attributed to fewer accessible emissive sites due to the enhanced crystal lengths arising from solvent annealing (Fig. 3b).

We conclude, in *stable* amorphous and annealed **HBDPP** films and *stable* seeded and annealed **BBDPP** films, quenching is influenced by Δ*G* for electron transfer, nitroaromatic vapour pressure and accessibility of emissive sites. In the other films examined, caution *must* be employed in assigning the origins of fluorescence quenching as being entirely due to charge transfer processes involving nitroaromatics; annealing effects on film morphology as well as polymorphism *can* give rise to a reduction in fluorescence intensity upon exposure to nitroaromatic vapours. Nevertheless, in addressing these caveats (which are not necessarily unique to DPP thin films), fluorescence quenching of *stable* DPP thin films qualifies their application as optical sensors in the detection of nitroaromatic vapours.

CJM and MW acknowledge EPSRC for funding under the First Grant Scheme EP/J011746/1. We thank the NCS at the University of Southampton for crystallographic data on **BBDPP**.

Notes and references

[a] *School of Science, University of the West of Scotland, Paisley, UK; Fax: 44 1418483204; Tel: 441418483210; E-mail: callum.mchugh@uws.ac.uk andrew.mclean@uws.ac.uk*
[b] *Pure and Applied Chemistry, University of Strathclyde, Glasgow, UK*
[c] *Photon Science Institute, University of Manchester, Manchester, UK*
[d] *School of Pharmacy, University of Reading, Reading, UK.*
[e] *Crystallografx Ltd., Milngavie, Glasgow, UK.*

† Electronic Supplementary Information (ESI) available: Full analysis of reported compounds and thin films. See DOI: 10.1039/b000000x/

1 J. Yinon, *Anal. Chem.*, 2003, 75, 99a.
2 S. Singh, *J. Hazard. Mater.*, 2007, 144, 15.
3 M. E. Germain and M. J. Knapp, *Chem. Soc. Rev.*, 2009, 38, 2543.
4 S. W. Thomas, G. D. Joly and T. M. Swager, *Chem. Rev.*, 2007, 107, 1339.
5 J. Yang and T. M. Swager, *J. Am. Chem. Soc.*, 1998, 120, 11864.
6 J. C. Ho, J. A. Rowehl and V. Bulovic, *Microsystems Technology Laboratories Annual Research Report*, 2009,
7 J. Calvo-Castro, M. Warzecha, A. R. Kennedy, C. J. McHugh and A. J. McLean, *Cryst. Growth. Des*, 2014, 14, 4849.
8 F. C. Spano, *Acc. Chem. Res.*, 2010, 43, 429.
9 M. Marshall and J. C. Oxley, *Aspects of Explosives Detection*, *Elsevier*, 2009.
10 S. Roy, A. K. Katiyar, S. P. Mondal, S. K. Ray and K. Biradha, *Appl. Mater. Interfaces.*, 2014, 6, 11493
11 C. Vijayakumar, G. Tobin, W. Schmitt, M. J. Kim and M. Takeuchi, *Chem. Commun.*, 2010, 46, 874.
12 C. F. Macrae, P. R. Edgington, P. McCabe, E. Pidcock, G. P. Shields, R. Taylor, M. Towler and J. van de Streek, *J. Appl. Cryst.*, 2006, 39, 453.
13. C. Wang, D. Huanli, H. Wenping, L. Yunqi and Z. Daoben, *Chem. Rev.*, 2012, 112, 2208.